



## CFD modeling of unsteady fluid flow and mass transfer in spacer-filled membrane modules

S. M. F. Hasani\*, M. Shakaib, M. Mahmood

*Department of Mechanical Engineering, N.E.D. University of Engineering and Technology*

*Karachi-75270, Pakistan*

*email: cmed@neduet.edu.pk, fhasani@neduet.edu.pk*

Received 15 September 2008; Accepted 14 July 2009

---

### ABSTRACT

The CFD simulations in spacer-filled membrane modules reveal complex fluid structure in diamond-type spacers as flow directional changes are seen due to inclined spacer filaments. Despite this complex fluid behavior the flow remains steady for the Reynolds number considered in this study. However, the flow in a parallel-type spacer earlier thought to be less complicated has shown three dimensionality as well as time dependency. Due to this transient nature, the flow becomes asymmetric with flapping motion. The eddies appear immediately behind the transverse filaments, grow in size and finally dissipate in the center of the filaments. The flow unsteadiness also causes the shear and mass transfer rates to vary in time and major fluctuations are seen in the center of the spacer filaments which may be useful in the periodic removal of foulants from membrane surfaces, thus improving the process efficiency.

**Keywords:** CFD; Membrane; Spacer; Shear rates; Mass transfer

---

### 1. Introduction

Membrane processes such as reverse osmosis, and nanofiltration are commonly used for desalination and other water treatment applications. Out of the variety of module configurations available for these processes, spiral wound type is most commonly used. The main advantage being that this type offers higher packing density at a much reduced module construction cost. Due to its importance in membrane applications, considerable design improvements have taken place over the years to enhance its performance. One particular component of the module that has received much attention is feed spacer. Bartels et al. [1] provide a detailed account of the design developments in spiral wound modules. Feed spacers in spiral wound membrane modules play an important role as they not only provide channel for feed flow but also create turbulence which promote mixing and reduce membrane fouling.

A number of experimental and numerical studies have appeared in literature in recent years. Schwinge et al. [2] studied the effect of spacer filaments on flow patterns using a CFD code. The work showed that flow becomes transient showing unsteady movements when Reynolds number is increased above 300. In another paper Schwinge et al. [3] found that transition to unsteady flow occurs between Reynolds number of 200 and 800 depending on spacer configuration. Ranade and Kumar [4] compared flow structure in spacer-filled flat and annular channels and concluded that fluid dynamics in two channels was not significantly different while secondary flows created by spacers were much stronger than those due to channel curvature. Koutsou et al. [5] studied the effect of Schmidt number on mass transfer rates in membrane feed channels for various spacers. Koutsou et al. [6] in another work performed direct numerical simulations in spacer-filled channels at different Reynolds numbers and compared them on the basis of wall shear stress distribution and pressure drop. Santos et al. [7] performed 3d simulations for

---

\*Corresponding author.

flow and mass transfer in flow-aligned diamond spacers and showed that critical value of Reynolds number for transient flows in membrane channels significantly depends on the spacer geometry. The work also showed that the effect of longitudinal filaments is insignificant on flow profiles and instabilities in spacer-filled channels. The effect of longitudinal filaments was not therefore considered for mass transfer cases in their paper. Fimbres-Weihs and Wiley [8] compared the concentration profiles obtained through 3d simulations with ones obtained using 2d analysis and reported that mass transfer rates were under-predicted in 2d simulations. Li et al. [9, 10] compared spacer performance based on average Sherwood and Power numbers. The modeling procedure in these papers however was not made clear particularly how periodic boundary conditions were applied to their problem. Li et al. [11] in another paper found that both woven and non-woven spacers perform equally well. Recently we [12, 13] studied the effect of spacer geometry on flow and concentration patterns in the membrane feed channels in the Reynolds number range between 10 and 200. This paper is an extension of our previous work and it gives a better insight into the flow structures and concentration patterns for an increased Reynolds number of upto 400 which is often the range encountered in most practical applications.

## 2. Modeling procedure and details

The flow and concentration patterns are obtained for two types of spacers: the diamond and the parallel spacers. Both spacers have two set of filaments; in a diamond spacer one set of filaments overlay upon another in different orientations on two different planes while in a parallel spacer a set of thin cross filaments is transversely connected to thick axial filaments. For both types of spacers the flow is periodic and flow entering the channel through one cell is similar to the flow that enters through the adjacent cell (in  $z$ -direction). In the main flow direction ( $x$ -direction) however the entry length is around 3–5 filaments [11]. The computational domain in this work is therefore restricted to one top/thick filament and six bottom/thin filaments for the diamond and parallel spacers as can be seen in Figs. 1(a) and (b).

In the diamond spacer vertical surfaces parallel to top filament are periodic surfaces while wall boundary conditions are defined for the axial filaments in the parallel spacer. For both spacer types:

1. Mass flow rate is specified in the  $x$ -direction at the inlet. The solute mass fraction  $c_0$  of fluid at inlet is zero. Mass flow rates are adjusted to obtain the desired value of Reynolds number.

2. The spacing between consecutive filaments is chosen to be 2 mm whereas the channel height is set to 1 mm.
3. The top and bottom membrane surfaces are assumed to be impermeable walls and are set to a mass fraction value  $c_w$  of 1. The assumption to treat membrane as an impermeable wall is satisfactory since in most of the membrane processes the feed velocity is at least 3 orders of magnitude higher when compared to permeation velocity.

The spacer geometry is created and meshed in Gambit 2.1.6 as shown in Fig. 2. The mesh consists of hexahedral and wedge type cells and is refined near the filaments and near the membrane (top and bottom) surfaces due to high velocity and concentration gradients. It is found that around 800,000 cells are sufficient for the range of Reynolds number considered in this paper. The difference in mass transfer coefficient and shear stress is found to be less than 3% when 800,000 and 1,450,000 cells are used respectively for parallel spacer at a Reynolds number of 400. The typical values of Schmidt number of the fluids in most of the membrane processes is commonly greater than 500. The higher values of Schmidt number however leads to significantly steep concentration gradients near the membrane wall. This necessitates extremely fine grid for accurate results thus increasing the computational time and cost. Therefore for modeling purpose a relatively lower value of Schmidt number of 100 is used for simulations in this paper. The governing equations are continuity, momentum and concentration equations which are solved using pressure based segregated solver of CFD code FLUENT 6.3. The discretization of momentum equation and concentration equation is carried out using QUICK and Power Law schemes respectively whereas pressure-velocity coupling is provided through SIMPLEC algorithm. The unsteady simulations are conducted using a time step of 0.0001 s and second order accurate formulation. In each time step, 20 iterations are specified in which the residuals of continuity, velocity and mass fraction (concentration) dropped around one order of magnitude indicating the convergence. Simulations are performed in parallel mode utilizing 12 nodes with 3 GHz dual processors. For the purpose of evaluation friction factors and Sherwood numbers are also obtained from pressure drop and mass transfer coefficient values of CFD results. The comparison is then made with the experimental work of Schock and Miquel [14] who developed following correlations for diamond spacer:

$$f = 6.23Re^{-0.3} \quad (1)$$

$$Sh = 0.065Re^{0.875}Sc^{0.25} \quad (2)$$

The definitions of Reynolds number  $Re$ , friction factor  $f$ , Sherwood number  $Sh$  and Schmidt number  $Sc$  are same as defined in reference [14]:

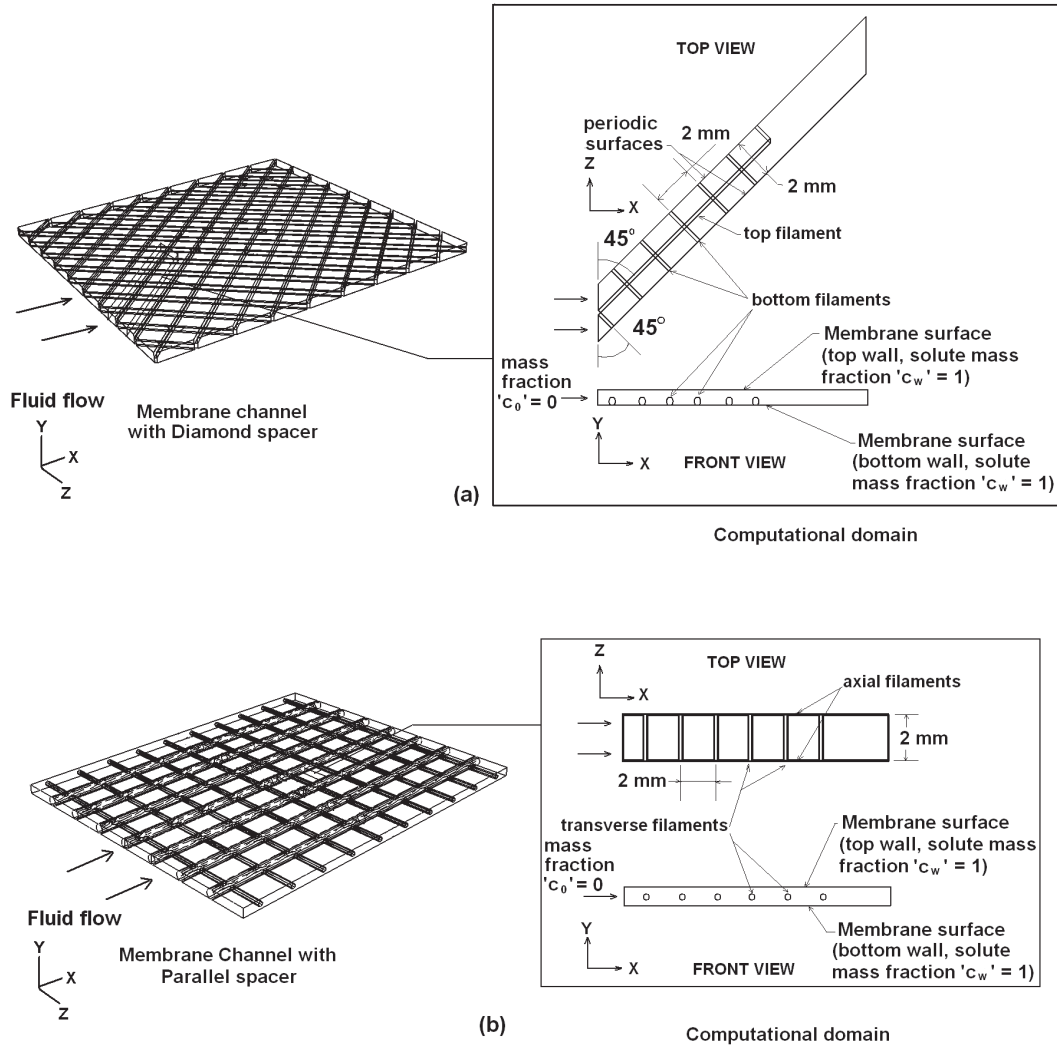


Fig. 1. Schematic and computational domains for (a) diamond spacer (b) parallel spacer.

$$Re = \frac{u_{av} d_h}{\nu} \tag{3}$$

where

$$u_{av} = \frac{m}{\rho A_{eff}} \tag{4}$$

$$d_h = \frac{4 \times \text{Volume of flow channel}}{\text{Wetted surface}} \tag{5}$$

$$f = \frac{2\Delta P d_h}{L \rho u_{av}^2} \tag{6}$$

$$Sh = \frac{k d_h}{D} \tag{7}$$

$$Sc = \frac{\nu}{D} \tag{8}$$

In Eqs. (3)–(8)  $d_h$  is hydraulic diameter,  $u_{av}$  is average velocity,  $m$  is mass flow rate,  $A_{eff}$  is effective area,  $\rho$  is density,  $\nu$  is kinematic viscosity,  $D$  is diffusion coefficient,  $L$  is distance and  $\Delta P$  is the pressure drop between any two filaments.

The present numerical results are also compared with the recent work of Koutsou et al. [5]. The results are compared with the correlation given in Eq.(9) which was determined for a spacer that resembles the diamond spacer considered in this work.

$$Sh_d = 0.14 Re_d^{0.64} Sc^{0.42} \tag{9}$$

where  $Re_d$  and  $Sh_d$  are Reynolds number and Sherwood number based on diameter  $d$  of the filaments

$$Re_d = \frac{u_{av} d}{\nu} \tag{10}$$

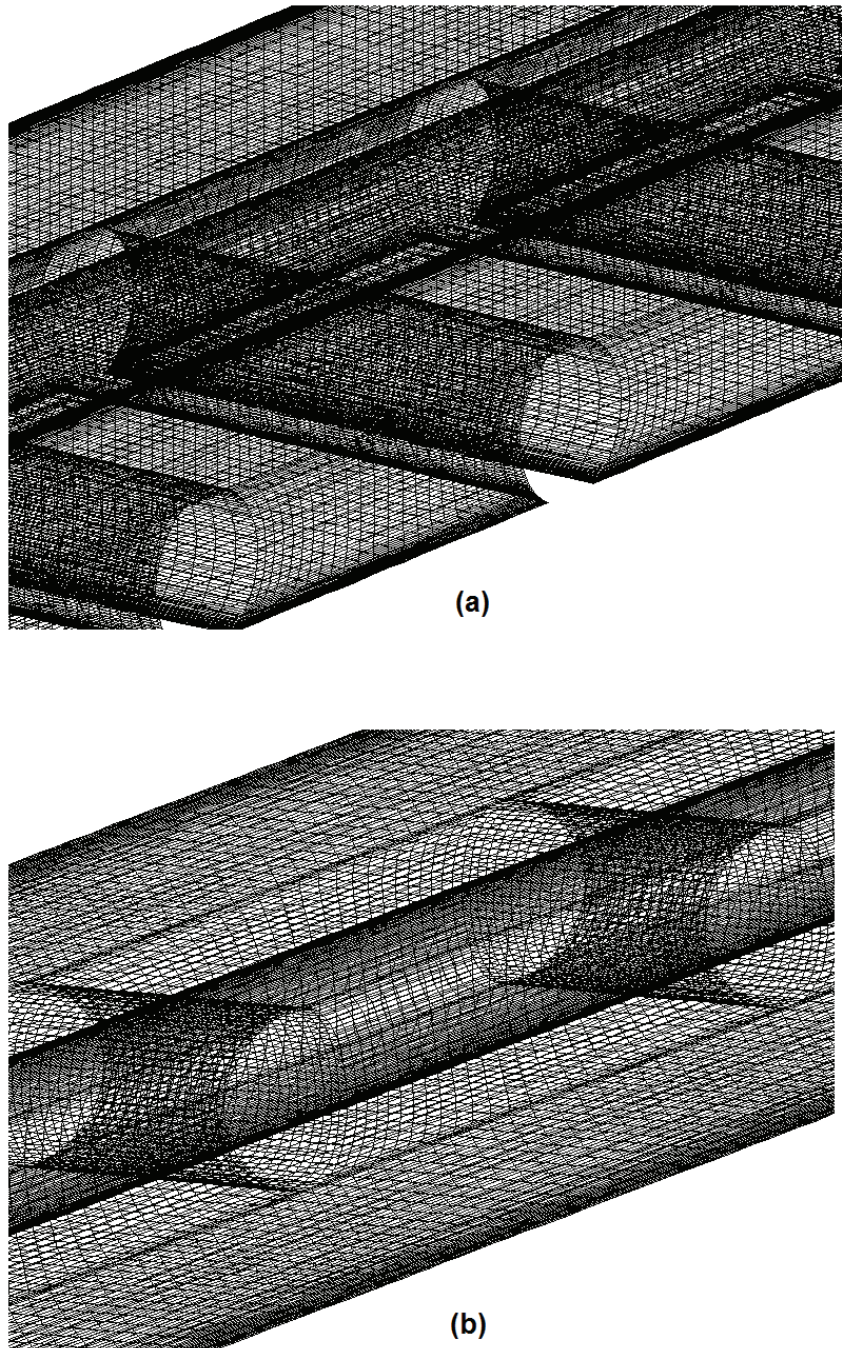


Fig. 2. Computational grid for (a) diamond spacer (b) parallel spacer.

$$Sh_d = \frac{kd}{D} \quad (11)$$

Since entrance effects are considerable for first few filaments and values of pressure drop and mass transfer rates are significantly higher at the inlet, the results in terms of shear stress, velocity profiles are presented for the last two filaments. Similarly the measurement of pressure drop  $\Delta P$

and mass transfer coefficient  $k$  for determining the friction factor and average Sherwood number for comparison with experimental results is made for the last two filaments.

### 3. Results and discussions

The flow fields in diamond and parallel spacers are shown in Fig. 3 with the help of path lines. It can be seen

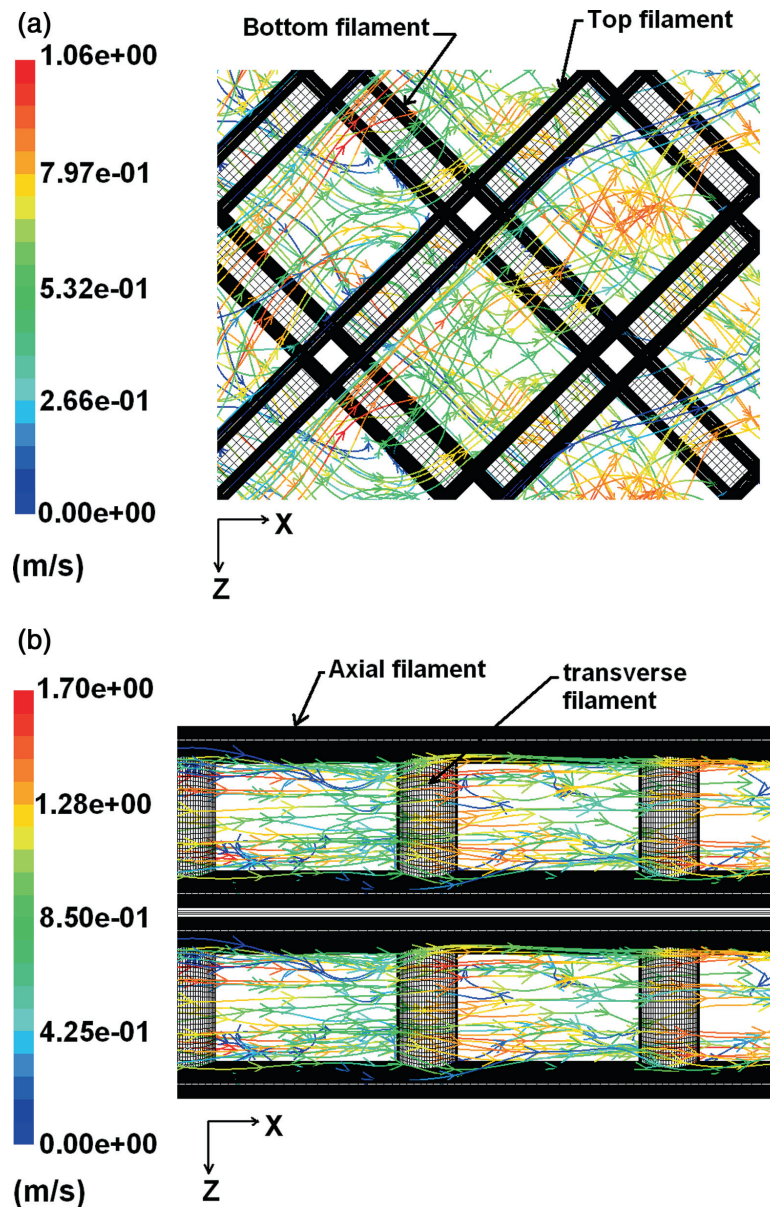


Fig. 3. Flow pattern in (a) diamond spacer (b) parallel spacer,  $Re = 400$ .

that the flow path is significantly different for the two spacers which ultimately result in different shear stress distributions and mass transfer coefficients. In a diamond spacer the flow directional changes are more prominent as portions of fluid moves above and beneath the bottom and top inclined filaments in the main flow direction. In addition some path lines are also seen almost aligned with the filaments indicating that portions of fluid get itself aligned with the filaments in an otherwise chaotic flow environment. The flow pattern in a parallel spacer, on the other hand is relatively simple and the fluid splits equally at the transverse filament flowing above and below the filaments

in the  $x$ -direction. Near the axial filaments however some deflection in flow direction can be noticed due to combined filament curvature and boundary layer effects. Figure 4 shows contours of mass transfer coefficient and shear stress on bottom membrane surface of a diamond spacer. From this figure it can be generally seen that higher shear stresses lead to higher values of mass transfer coefficients and lower values of shear rates result in lower values of mass transfer coefficient except at few portions (such as zones 1 and 2 in Fig. 4). One of these locations (zone 1) is where shear stress values are low while mass transfer rates are high. The mass transfer rates increase

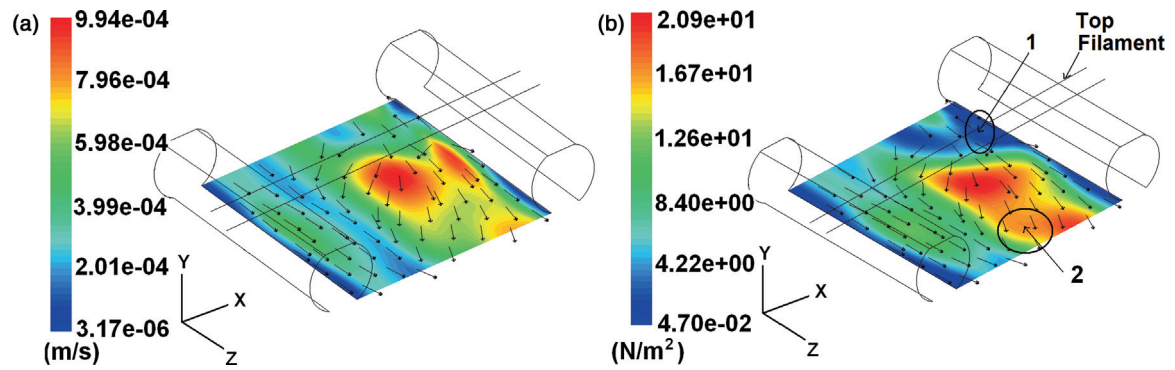


Fig. 4. Contours of (a) mass transfer coefficient and (b) shear stress in diamond spacer ( $Re = 400$ ).

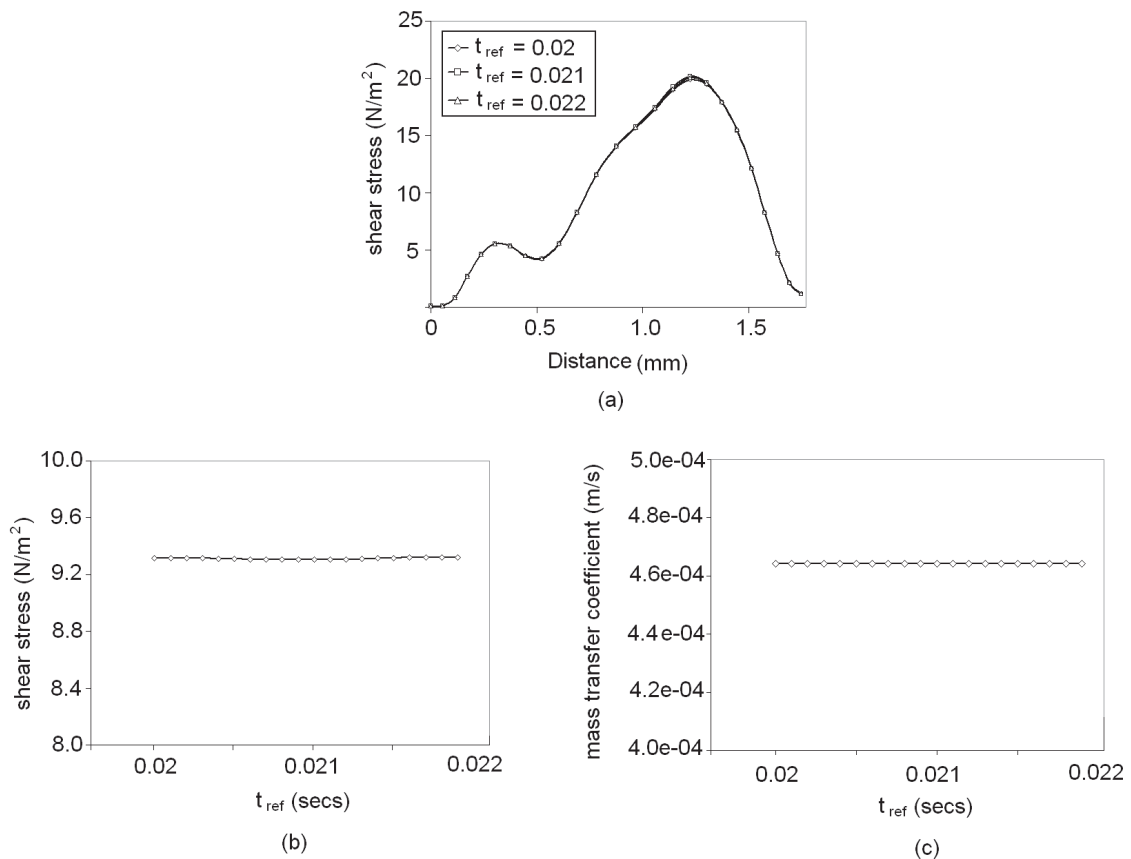


Fig. 5. (a) Shear stress variation on the bottom wall and average value of (b) shear stress and (c) mass transfer coefficient with respect to time ( $Re = 400$ ).

in this zone due to disruption of concentration polarization layer from scouring effect of flow recirculation. The other location is one with high shear stress (zone 2) where fluid is diverted in the z-direction with high velocity due to bottom filament obstacle. The mass transfer coefficient values do not rise in this zone and its higher value remains restricted in the region below the top filament. The spacers are also examined on the basis of flow instabilities. These

flow instabilities can bring periodic change in shear stress and mass transfer rates near the membrane surfaces which can be useful for the filtration process. The critical value for transition to unsteady flow significantly depends on spacer geometry and varies from 75–800 depending on spacer type, filament spacing and thickness [3, 6, 7]. In a diamond spacer it is found that even though the velocity profile is comparatively complex than a parallel spacer,

yet it is almost free from flow fluctuations. The unsteady simulation at a time step of 0.0001 secs showed negligible variation of parameters such as velocity, shear stress with respect to time upto a Reynolds number of 400. It can be seen in Fig. 5 (a) that shear stress plots on the bottom wall of the periodic plane overlap at different time steps except in the vicinity of maximum value where slight differences can be found. In a similar manner it is observed in Figs. 5 (b) and (c) that the variation of average values of shear stress and mass transfer coefficient on the bottom surface are insignificant (less than 0.2 %).

The flow patterns in a parallel spacer however vary considerably with time at the Reynolds number value of 400. The time-dependent flow behavior between the last two filaments of parallel spacer is shown at different time steps in Fig. 6. For steady flow in a parallel spacer the high velocity region above and below the filaments and recirculation wake remains symmetric. When the flow becomes unsteady the high velocity and recirculation zones become asymmetric causing flow oscillations (Fig. 6). These oscillations give rise to the formation of small vortices in the recirculation zone behind the transverse filaments; two small eddies appear at the junction of high velocity and recirculation regions. These eddies appear near the transverse filament, grow in size while moving in the flow direction and die somewhere in the center of the two transverse filaments. The three dimensionality of flow in a parallel spacer is shown with the help of Fig. 7 where cross-sections in the  $x$ - $y$  plane are cut at various distances from the vertical plane chosen to be the mid-plane between two axial filaments. It can be seen that the

size of vortex in the upper region near the transverse filament reduces when it is observed at planes 0.1 and 0.2 mm from the central plane. This vortex is no more present at plane that is located at a distance of 0.3 mm from central plane. The vortex which is seen in the lower region in Fig. 7 (a) is found to be shifted when it is viewed at planes 0.1 and 0.2 mm (Figs. 7 (b) and (c)). This vortex again is not observed at a plane which is at a distance of 0.3 mm from the center. The size of main recirculation region is also very short at this plane. In addition to main recirculation behind the filament, recirculation is also observed at the membrane surface which is more obvious in Fig. 7 (c). The size and strength of high velocity region is found to be greater at the planes which are at distances of 0.2 and 0.3 mm respectively. This occurs due to curved surface of the axial filaments which allow the high velocity fluid to expand and divide into two parts as it leaves the transverse filament and moves ahead. The variation of shear stress and mass transfer coefficient for a single spacer mesh cell along its length and width is shown in Fig. 8. The shear stress and mass transfer coefficient between two transverse filaments are observed along Line A (Figs. 8 (a) and (b)) while the same are monitored between the axial filaments along Line B (Figs. 8(c) and (d)). The length of Line A is 2 mm which is equal to center-to-center distance between transverse filaments while length of line B is 1.5 mm which is less than distance between axial filaments as some portion of membrane surface is covered by axial filaments. It can be seen that at all time steps maximum values of shear stress and mass transfer coefficient lie almost above the transverse filaments. The

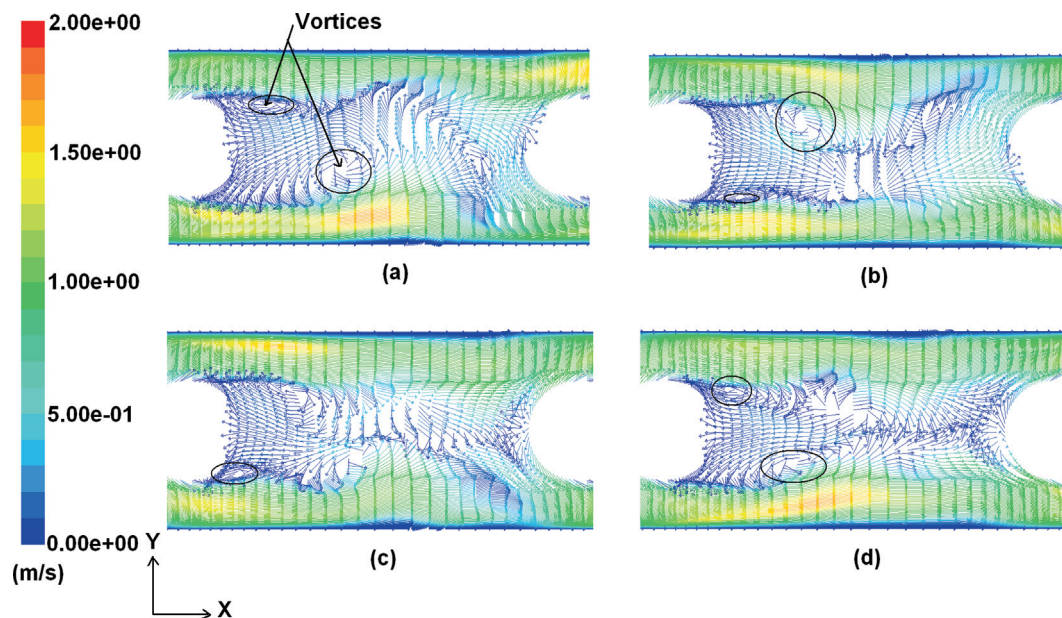


Fig. 6. Velocity vectors in parallel spacer at (a)  $t_{\text{ref}} = 0.041$  (b)  $t_{\text{ref}} = 0.042$  (c)  $t_{\text{ref}} = 0.043$  (d)  $t_{\text{ref}} = 0.044$  seconds ( $Re = 400$ ).

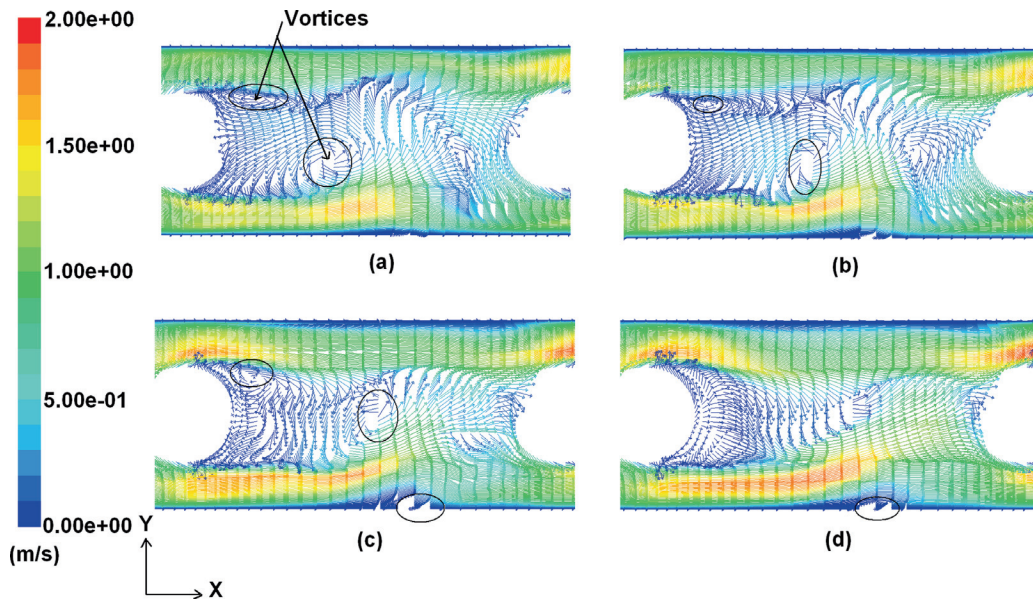


Fig. 7. Velocity vectors at a distance of (a) 0 mm (b) 0.1 mm (c) 0.2 mm (d) 0.3 mm from a plane in center of two axial filaments ( $Re = 400$ ).

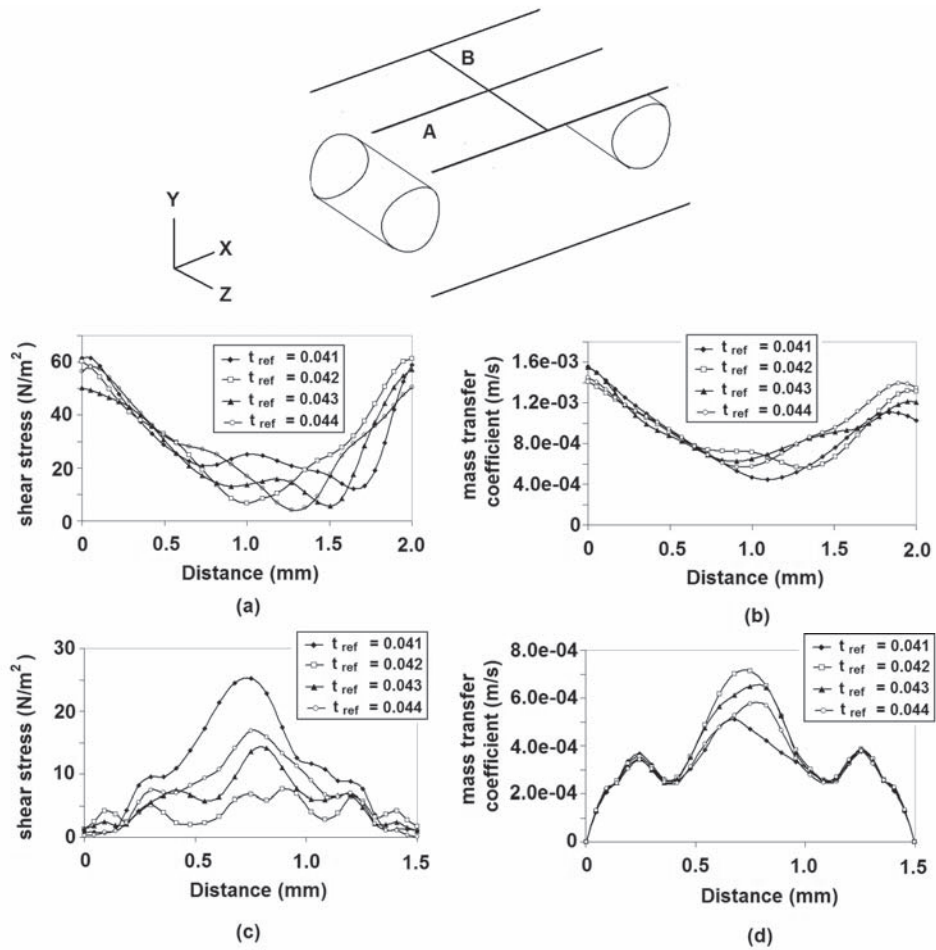


Fig. 8. Distribution of shear stress and mass transfer coefficient between (a, b) transverse filaments (c, d) axial filaments ( $Re = 400$ ).

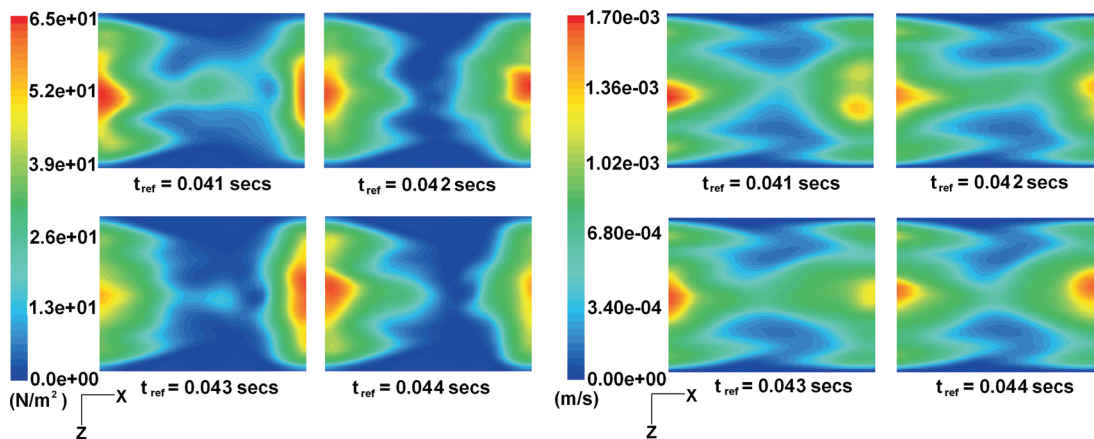


Fig. 9. Contours of shear stress and mass transfer coefficient on top wall of parallel spacer at different time steps (Re = 400).

fluctuations are more somewhere in center of these filaments. The plot of shear stress and mass transfer coefficient between axial filaments show that the absolute values of shear and mass transfer rates and their fluctuations are maximum in the center of the filaments. These values along with their fluctuations reduce and vanish near the axial filaments. The contours in Fig. 9 further describe the variation of shear stress and mass transfer coefficient at different time steps. It can be seen that shear stress and mass transfer coefficient remains high above the transverse filaments for all time steps. Since flapping motions occur, the high velocity fluid gets attached and detached from the membrane surface at frequent intervals. In the central portion, the value of shear stress therefore rises at one instant and falls at the other instant. This pattern of varying shear stress and mass transfer coefficient can be useful for membrane processes, as the fouling agents get periodically removed from membrane surface, which can reduce the membrane cleaning costs. The detachment of high velocity fluid region often leads to separation and flow recirculation. This recirculation though causes lower shear rates but enhances the mass transfer rates in the central portion. The mass transfer coefficients are thus found to be increasing and decreasing in a similar manner but their distribution is more uniform when compared to shear stress. The parallel spacer is also compared on the average shear stress and mass transfer coefficient basis with the diamond spacer. The comparison showed that for parallel spacer shear stress and mass transfer coefficient are 100 % and 35 % higher respectively than the diamond type spacer.

Since experimental results are not generated in this paper, validation of the numerical results of this study is made by comparing them with the experiments of Schock and Miquel [14] and Koutsou et al. [5] in which correlations were developed for friction factor and Sherwood number for diamond type spacers.

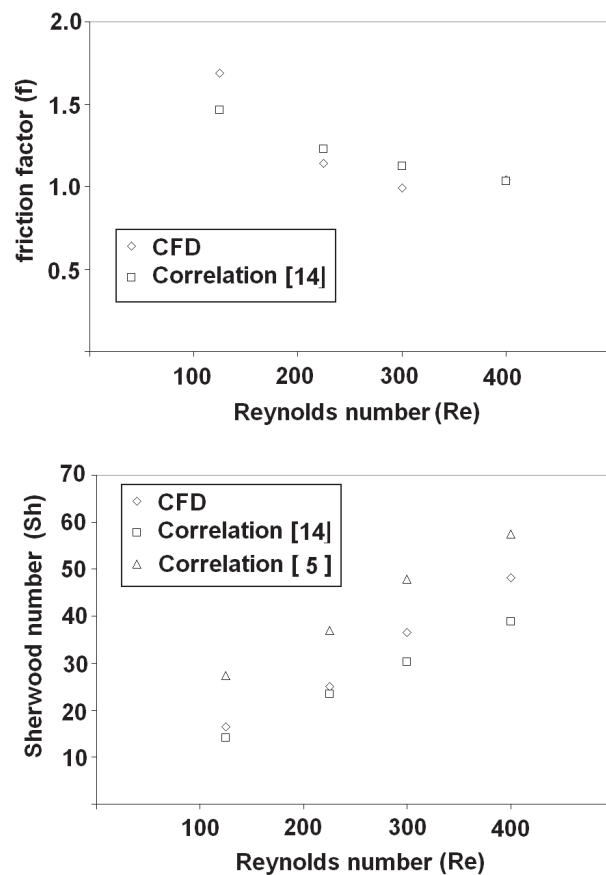


Fig. 10. Comparison of numerical and experimental results [5, 14].

The comparison for diamond spacer in this study which resembles with the spacers in references [5, 14] in Fig. 10 shows that satisfactory agreement exists between present CFD results and experiments as differences are around 25 % and 50 % respectively with the work of Schock and

Miquel [14] and Koutsou et al. [5]. Perfect agreement between simulations and experiments is unexpected due to uncertainties and approximations included in both the techniques. For example the spacer filament shape is assumed of uniform cross-section for modeling purposes whereas in real spacers the cross-section may not be uniform due to manufacturing defects. Similarly the accuracy of measuring instruments can affect the pressure drop and mass transfer rates. The other possible sources of differences could be the modeling procedure, the selection of numerical discretization schemes and assumptions such as the use of impermeable 'wall' boundary condition for the membrane surface. The above several reasons can lead to difference in CFD and experimental results at higher or even at lower Reynolds number.

#### 4. Conclusions

CFD analysis in membrane channels with spacers show that flow patterns, distribution of shear stress and mass transfer coefficient largely depends on spacer geometry. The flow in the investigated diamond spacer geometry of this study remained steady upto a Reynolds number of 400. The flow in the parallel spacer is found to be transient at the same Reynolds number and vortices emerge, move and disappear at frequent intervals behind the filaments. Significant three dimensional effects are also seen in the membrane channel. The size of vortices and the main recirculation regions reduce near the axial filaments. The parallel spacer under the test conditions used in this study depicted superior performance as mass transfer rates are higher and unsteadiness in flow causes variation in mass transfer rates at the membrane surface which can be beneficial for membrane filtration processes. For diamond spacers, however, better designs could be possible by varying the geometric parameters such as filament spacing and flow attack angle which not only provide directional flow changes but also introduce flow instabilities. Finally, fair agreement is found between present numerical results with published experimental correlations.

#### Acknowledgments

The authors acknowledge the support provided by High Performance Computing Centre at the NED University of Engineering and Technology, Karachi and the Higher Education Commission (HEC) of Pakistan.

#### Nomenclature

$A_{eff}$	Effective area (m <sup>2</sup> )
$c_0$	mass fraction at inlet (kg/kg)
$c_w$	mass fraction at membrane surface (kg/kg)
$d$	filament diameter (m)
$d_h$	hydraulic diameter (m)
$D$	diffusion coefficient (m <sup>2</sup> /s)
$f$	friction factor
$k$	mass transfer coefficient (m/s)
$L$	Length (m) (distance between filaments)
$m$	mass flow rate (kg/s)
$Re$	Reynolds Number (based on hydraulic diameter)
$Re_d$	Reynolds Number (based on filament diameter)
$Sc$	Schmidt Number
$Sh$	Sherwood Number (based on hydraulic diameter)
$Sh_d$	Sherwood Number (based on filament diameter)
$u_{av}$	average velocity (m/s)
$\nu$	kinematic viscosity (m <sup>2</sup> /s)
$\Delta P$	pressure drop (Pa) (measured between last two filaments)
$\rho$	density (kg/m <sup>3</sup> )

#### References

- [1] C. Bartels, M. Hirose and H. Fujioka, *Desalination* 221 (2008) 207–214.
- [2] J. Schwinge, D.E. Wiley and D.F. Fletcher, *Desalination* 146 (2002) 195–201.
- [3] J. Schwinge, D.E. Wiley and D.F. Fletcher, *Ind. Eng. Chem. Res.* 42 (2003) 4962–4977.
- [4] V.V. Ranade and A. Kumar, *Desalination* 191 (2006) 236–244.
- [5] C.P. Koutsou, S.G. Yiantsios and A.J. Karabelas, *J. Membr. Sci.* 326 (2009) 234–251.
- [6] C.P. Koutsou, S.G. Yiantsios and A.J. Karabelas, *J. Membr. Sci.* 291 (2007) 53–69.
- [7] J.L.C. Santos, V.M. Geraldes, S. Velizarov and J.G. Crespo, *J. Membr. Sci.* 305 (2007) 103–117.
- [8] G.A. Fimbres-Weihs and D.E. Wiley, *J. Membr. Sci.* 306 (2007) 228–243.
- [9] F. Li, W. Meindersma, A.B. de Haan and T. Reith, *Desalination* 146 (2002) 209–212.
- [10] F. Li, W. Meindersma, A.B. de Haan and T. Reith, *J. Membr. Sci.* 208 (2002) 289–302.
- [11] F. Li, W. Meindersma, A.B. de Haan and T. Reith, *J. Membr. Sci.* 232 (2004) 19–30.
- [12] M. Shakaib, S.M.F. Hasani and M. Mahmood, *J. Membr. Sci.* 297 (2007) 74–89.
- [13] M. Shakaib, S.M.F. Hasani and M. Mahmood, *J. Membr. Sci.* 326 (2009) 270–284.
- [14] G. Schock and A. Miquel, *Desalination* 64 (1987) 339–352.